RSC Advances

ROYAL SOCIETY OF CHEMISTRY

www.rsc.org/advances

Tuneable Thermopower and Thermal Conductivity in Lu Doped In_2O_3

BeiBei Zhu[a], Ruoming Tian[a*], Tianshu Zhang[a*], Richard Donelson[b], Thiam Teck Tan[a], Yu Wang[c] and Sean Li[a]

[a]School of Materials Science and Engineering, University of New South Wales, NSW 2052, Australia

[b]CSIRO, Clayton South, VIC 3162, Australia

[c] XRD Laboratory, Chemical Sciences, University of New South Wales, NSW 2052, Australia

[*]Corresponding author: r.tian@unsw.edu.au, and 13335516617@163.com

Abstract

Lu-doped polycrystalline $(In_{1-x}Lu_x)_2O_3$ (x=0, 0.025, 0.05, 0.10, 0.15) materials were prepared using co-precipitation method followed by spark plasma sintering processing. The large and heavy Lu^{3+} was strategically selected to replace In^{3+} for lowering the thermal conductivity with minimal interruption of electronic structure of the systems. The as-synthesized materials have microstructure with average grain size of 200-400nm and ~90% of the theoretical mass density. Lu doping was found to simultaneously increase the thermopower and electrical resistivity of In_2O_3 due to the drastically decreased carrier concentration, while the thermal conductivity can be reduced remarkably through Lu doping.

KEYWORDS

In_2O_3; Co-precipitation; Raman spectroscopy; Thermopower; Thermal conductivity

1. Introduction

Thermoelectric conversion has become an important approach to harvest waste heat to generate useful electricity. It has a variety of applications in automotive industry, solar thermal plant and deep-space stations[1]. For these applications, it requires materials to not only possess a high thermoelectric figure of merit, but also be abundant and non-toxic to satisfy the environmental concern.

Traditional alloy materials, such as Bi_2Te_3 and PbTe, have relatively better performance compared with the oxide-based materials in a lower temperature range. However, their chemical and thermal stabilities at high temperature as well as environmental compatibility are a great concern. For the thermoelectric modules, both p-type and n-type thermoelectric materials are the essential components to form the p-n junctions, but the current development of n-type oxides materials is a bit far behind that of p-type materials.

In_2O_3 is considered as one of promising n-type oxide-based materials due to its good electrical conductivity. Previous study shows that the carrier concentration of In_2O_3 could be influenced by either oxygen vacancies or indium interstitials [2-4]. In addition to these intrinsic factors, doping technology has been used as an alternative route to tailor the thermoelectric parameters of this material system from an extrinsic perspective. It is reported that Sn doping could remarkably increase the electrical conductivity, resulting in approximately 5 times higher than the power factor of the undoped counterpart[5]. Similarly, the substitution of Ce in the In site could produce a ZT as high as ~0.47 at 1223 K[6]. Although intensive studies have been implemented

to enhance the electrical conductivity *via* doping with tetravalent and pentavalent cations, the realization of low thermal conductivity and high thermopower in this particular material system remains a great challenge due to its relatively high carrier concentration[5-7].

Furthermore, the technique of sample preparation, such as co-precipitation, has also been experimentally proven to be an effective approach to produce homogeneous material[8] with nanostructures[9]. In the present work, we prepared Lu doped In_2O_3 compounds with a series of doping concentrations with the co-precipitation methodology followed by spark plasma sintering. The large and heavy element Lu^{3+} was strategically selected as the dopant to replace In^{3+}. It is expected that such substitution would form additional phonon scattering centers over the grain boundaries at the atomic scale with a minimal interruption in the electronic structure of the system[10], thus enhancing the thermoelectric performance of the materials.

2. Experimental Section

Lu doped In_2O_3 powders were synthesized *via* co-precipitation method using ammonia as precipitant. Aqua solutions of $InCl_3$ and $LuCl_3$ were thoroughly mixed in the stoichiometric ratio. Ammonia solution was slowly added into the mixed salt solution and the pH value was controlled in 11. The resultant suspension was kept stirring at room temperature for 20 min. Subsequently the suspension was homogenized overnight after the completion of precipitation and filtered with a centrifuge (Thermo Scientific). The precipitates were washed four times with distill

water to remove the extra chloride ion before drying at 80°C for 12h. The dried precursor was calcined at 700°C in air for 3 h to obtain the single phase powder. The sintering process was carried out in spark plasma sintering system (Dr. Sinter SPS System). The calcined powders were placed into a graphite die with the diameter of 20 mm and sintered at 1243 K for 5 min under a uniaxial pressure of 50 MPa. The sintered pellets were annealed at 1223 K for 3 h in air to remove the graphite foil on the surface.

Phase characterization was carried out by X-ray diffractometer (Panalytical) with Cu K_α radiation. Microstructure was analyzed using field-emission scanning electron microscopy (NanoSEM 230). Phonon excitation was characterized using a Raman spectrometer (Renishaw Raman Microscope) with Ar ion laser (514 nm). Band gap energy of the samples was measured by UV-VIS spectrophotometer (PerkinElmer Lambda 950). Carrier concentration and mobility were determined by using a Hall measurement system (HL5500PC). The electrical resistivity and thermopower as a function of temperature were measured from 373 K to 973 K with high temperature Seebeck probe system (ULVAC-RIKO ZEM-3, Japan). Thermal conductivity (κ) was calculated from the relation $\kappa(T)=D(T) \times C_p(T) \times d(T)$, where the thermal diffusivity (D), specific heat (C_p) and density (d) as a function of temperature (T) were defined. D (T) was measured by using a laser flash apparatus (NETZSCH LFA 427). C_p (T) was measured by using a differential scanning calorimeter (NETZSCH DSC 404C). d was measured using the Archimedes method.

3. Results and Discussion

Table 1 presents the theoretical mass density and relative density. A unit cell of In_2O_3 contains of 32 In atoms and 48 oxygen atoms. Therefore, the doping dependence of theoretical mass density in the $(In_{1-x}Lu_x)_2O_3$ system is derived from the cell volume and the molecular formula [11, 12]:

$$d = \frac{32(1-x)M_{In}+32xM_{Lu}+48M_O}{N_A a^3 \times 10^{-24}} \quad \text{Equation 1}$$

where a is the lattice constant, N_A Avogadro number and M the atomic weight of the corresponding elements. The relative density of Lu doped In_2O_3 compounds is in the range of 89%-94%**.**

Fig. 1a shows that the SEM morphology of the undoped sample prepared by the co-precipitation and SPS processing. It shows the microstructure of the prepared materials with the average grain size of 200-400nm. The other Lu doped samples have similar microstructures and grain size to the undoped sample. For comparison, the undoped In_2O_3 sample prepared by the co-precipitation followed by pressure-less sintering is presented in Fig. 1b. It contains a large number of pores (~70% of theoretical maximum) and the grain size is around 1-5μm. This demonstrates that the combination of co-precipitation and SPS provides a facile approach to produce materials with relatively high density and smaller grains.

Fig. 2**a** and Fig. 2**b** show the temperature dependence of electrical resistivity and thermopower for the investigated samples. It is found that the doping of Lu remarkably enhanced the thermopower of In_2O_3 although it inevitably increased the electrical resistivity simultaneously. The thermopower of the sample containing 15%

Lu (x=0.15) is not included in Fig. 2b as it is out of the limitation of the instrument due to its large resistivity, the magnitude of resistivity at 373K is 6 orders larger than that of its undoped counterpart(Fig. 2a). Fig. 2c plots the resistivity and thermopower as a function of Lu concentration at different temperatures. It shows that the resistivity increased with increased Lu concentration. But the thermopower gradually increased from 254μV/K to 400μV/K at 973K, which was 60% higher than that of its undoped counterpart. The temperature dependent power factors of the samples are showed in Fig. 3. It shows that the power factor (PF) increases with increase of the temperature and the increase of doping concentration leads to the decrease of power factor, which is associated with the doping level dependence of electrical resistivity in the $(In_{1-x}Lu_x)_2O_3$ system.

The difference of the relative densities among the measured samples is less than 5%. Therefore, the variation in the resistivity and thermopower upon Lu doping may be caused by other factors. In order to further investigate the electrical transport mechanism of this material system, Hall Effect measurement was conducted and the results are listed in Table 2. It is found that electrical resistivity follows the opposite trend of carrier concentration, which decreases with the increase of Lu doping concentration, particularly when the Lu content exceeded 5% (x=0.05). For instance, the carrier concentrations in the samples containing 10% (x=0.10) and 15% (x=0.15) of Lu were about 3 to 4 order magnitude lower than that of the undoped sample at room temperature. This gives a rise of question in why these measurement results contradicts to our strategy thought at the beginning, which the substitution of Lu^{3+}

onto In^{3+} site should have a limit influence on the carrier concentration in the $(In_{1-x}Lu_x)_2O_3$ system. To reveal the mechanism of this phenomenon, we investigated the possibility from the intrinsic behavior first. It is noted that the band gap energy increased with increasing Lu content as shown in Fig. 4. This may make a partial contribution to the reduction of carrier concentration as the band gap widening increases the barrier height for the electrons to excite from the valence band to conduction band. Such a band gap energy dependence of carrier concentration can be calculated with the following equation

$$n \propto \exp(-\frac{E_g}{kT}), \quad \text{Equation 2}$$

where E_g is the band gap energy, k the Boltzmann constant and T the absolute temperature [13]. The calculation results show that the band gap widening results in the decrease of carrier concentration, which is 2 times lower than that of the In_2O_3. But this is still far from the one order magnitude lower in the carrier concentration induced by the Lu doping as measured in our experiments. It implies the involvement of other mechanisms. The Hall Effect measurement was carried out to study the influence of oxygen deficiency on the electrical transport properties. The samples were isothermally annealed in air, argon and nitrogen atmosphere at 1173K for 6 hours, respectively, to vary the concentrations of oxygen vacancies. The experimental results in Table 3 show that the annealing atmosphere has very limit influence on carrier concentration of the undoped samples while its influence on the doped sample (x=0.05) is significant. In addition, we have carried out the resistivity/thermopower measurement on the x=0.05 sample annealed in nitrogen atmosphere. The results are

shown in the supplementary document (Fig. S1), which demonstrates that the sample annealed in air has higher power factor than that annealed in N_2 in the entire range of temperatures.

Although the actual mechanism of Lu doping effects on carrier concentration has not been identified, the contribution from the variation of band gap energy and oxygen vacancy concentration induced by the Lu doping can be ruled out by our experimental results. We believe that the origin of this phenomenon is very complicated and it may be associated with electron or orbital reconstruction linked with the individual electronic structures of Lu^{3+} and In^{3+} as well as their local chemical environment related to O^{2-}. These will be investigated by X-ray Absorption Spectroscopy.

Fig. 5 shows the Raman spectra for all investigated samples, which consists of 6 Raman modes around 112, 133, 309, 368, 496 and 630 cm^{-1}. This is consistent with the previous reports[14]. It is found after Lu doping, Raman peaks shift to higher energies and become broader. The shift of Raman peak position and broadening are resulted from the dopant incorporation, which leads to the change of bonding strength and local chemical environment, thus influencing the lattice parameters[15]. Moreover, in Raman spectra, a few shoulders (*i.e.*, 496cm^{-1} and 630cm^{-1}) can be observed in the heavily doped samples (*i.e.*, x=0.1 and x=0.15) as indicated by the arrows in Fig. 5. As reference, similar characterisation was carried on the pure Lu_2O_3 sample and the result is included in Fig. 5. It can exclude the contribution from Lu_2O_3 phase.

Fig. 6 shows the XRD pattern of the as-synthesized $(In_{1-x}Lu_x)_2O_3$ materials, which are

single phase by referring to the standard In_2O_3 (ICSD-640179). It is also discernible that the diffraction peaks shift towards lower angles with increased Lu doping concentration, indicating the lattice expansion induced by the larger ionic radius of Lu ions [16]. The finding from XRD patterns was verified by Raman spectra (Fig. 5). It is interesting to note that the doping increases the full width at half maximum (FWHM) of XRD characteristic peaks (the Insert in Fig. 6). As aforementioned, all the samples have the similar grain size, thus the influence of grain size on the FWHM can be negligible in this case. On the other hand, the isostructural phenomenon of $(In_{1-x}Lu_x)_2O_3$ may be responsible for the broadening XRD peaks. The mechanism is still under investigation.

Fig. 7 plots the effects of Lu addition on the temperature dependence of thermal conductivity. It was found that the doping with 15% Lu lowered the thermal conductivity of In_2O_3 about 40% at near room temperature. As aforementioned, the difference of their relative densities is less than 5%, therefore, the influence of porosity on the thermal conductivity can be neglected in this case. For semiconductors, the total thermal conductivity consists of both electronic thermal conductivity (κ_e) and phonon (or lattice) thermal conductivity (κ_{ph}). The former is believed to be decreased with Lu doping due to the decreased carrier concentration as evidenced by the Hall Effect measurement. The latter can be influenced by the grain boundaries, doping-induced point defect scattering and impurities.

As aforesaid, all the SPS samples showed similar grain sizes due to the same synthesis condition, hence the contribution of grain boundaries to the lattice thermal

conductivity was considered to be equal to each other. On the other hand, for In_2O_3 based materials, the average phonon mean free path is estimated to be approximately 10Å[17] which is close to the lattice parameter. Therefore, the lattice thermal conductivity κ_{ph} may be significantly influenced by dopant induced phonon scattering due to the difference in their atomic mass between Lu (175g/cm^3) and In (115 g/cm^3). Although both electronic thermal conductivity and phonon thermal conductivity were decreased by the doping of Lu, the contribution from electrons was estimated to be less than 5% (by employing Wiedemann Franz law).

Fig. 8 plots the temperature dependence of ZT with different Lu doping level. It shows that the ZT decreases with the doping concentration, which is strongly related to the decrease of power factor (Fig. 3). Therefore, to achieve higher thermoelectric figure of merit, the $In_{2-2x}Lu_{2x}O_3$ ceramics should be further modified to possess high conductivity.

4. Conclusions

Lu doped $(In_{1-x}Lu_x)_2O_3$ (x=0, 0.025, 0.05, 0.10, 0.15) were synthesized using co-precipitation followed by SPS processing. Microstructure analysis indicated that the as-prepared samples have the average grain size of 200-400nm. The substitution of Lu^{3+} for In^{3+} resulted in a simultaneous increase of electrical resistivity and thermopower although they possess the same valence state. Hall Effect measurement demonstrated that the carrier concentration was drastically decreased with Lu doping, particularly when the Lu concentration was beyond 5%. The origin of this

phenomenon is complicated and needs to be further investigated. In addition, the thermal conductivity was found to be suppressed with Lu doping, which can be mainly attributed to the doping-defect phonon scattering.

Acknowledgements

The authors would like to acknowledge Australian Renewable Energy Agency (ARENA), Chinese Scholarship Council, Australian Research Council Project of DP0988687 and LP120200289, Baosteel for the financial supports in this research project**.**

References

1. Tritt, T.M. and M. Subramanian, *Thermoelectric materials, phenomena, and applications: A bird's eye view.* MRS bulletin, 2006. **31**(03): p. 188-198.
2. Walsh, A., et al., *Physical properties, intrinsic defects, and phase stability of indium sesquioxide.* Chemistry of Materials, 2009. **21**(20): p. 4962-4969.
3. Tomita, T., et al., *The origin of n-type conductivity in undoped In_2O_3.* Applied physics letters, 2005. **87**(5): p. 051911-051911-3.
4. De Wit, J.H.W., *Electrical properties of In_2O_3.* Journal of Solid State Chemistry, 1973. **8**(2): p. 142-149.
5. Guilmeau, E., et al., *Tuning the transport and thermoelectric properties of In_2O_3 bulk ceramics through doping at In-site.* Journal of applied physics, 2009. **106**(5): p. 053715-053715-7.
6. Liu, Y., et al., *High Temperature Transport Property of $In_{2-x}Ce_xO_3$ ($0 \leq x \leq 0.10$) Fine Grained Ceramics.* Journal of the American Ceramic Society, 2012. **95**(8): p. 2568-2572.
7. Bérardan, D., et al., *In_2O_3:Ge, a promising n-type thermoelectric oxide composite.* Solid State Communications, 2008. **146**(1-2): p. 97-101.
8. Luo, W. and J. Dahn, *Comparative study of Li $[Co_{1-z}Al_z]O_2$ prepared by solid-state and co-precipitation methods.* Electrochimica Acta, 2009. **54**(20): p. 4655-4661.
9. Yu, D., et al., *Synthesis of ITO nanowires and nanorods with corundum structure by a co-precipitation-anneal method.* Materials Letters, 2004. **58**(1): p. 84-87.
10. Biswas, K., et al., *High-performance bulk thermoelectrics with all-scale hierarchical architectures.* Nature, 2012. **489**(7416): p. 414-418.
11. Riess, I., D. Braunshtein, and D. Tannhauser, *Density and Ionic Conductivity of Sintered $(CeO_2)_{0.82}(GdO_{1.5})_{0.18}$.* Journal of the American Ceramic Society, 2006. **64**(8): p. 479-485.
12. Gonzalez, G., et al., *Defect structure studies of bulk and nano-indium-tin oxide.* Journal of applied physics, 2004. **96**(7): p. 3912-3920.
13. de Wit, J.H.W., *The high temperature behavior of In2O3.* Journal of Solid State Chemistry, 1975. **13**(3): p. 192-200.
14. Gan, J., et al., *Oxygen vacancies promoting photoelectrochemical performance of In_2O_3 nanocubes.* Scientific reports, 2013. **3**.
15. Farvid, S.S., M. Hegde, and P.V. Radovanovic, *Influence of the Host Lattice Electronic Structure on Dilute Magnetic Interactions in Polymorphic Cr (III)-Doped In2O3 Nanocrystals.* Chemistry of Materials, 2013. **25**(2): p. 233-244.
16. Shannon, R.D., Acta Crystallogr, Sect. A, 1976. **32**: p. 751.
17. Ashida, T., et al., *Thermal transport properties of polycrystalline tin-doped indium oxide films.* Journal of applied physics, 2009. **105**(7): p. 073709-073709-4.

Figure captions

Table 1 Mass densities and calculated relative densities for Lu-doped In_2O_3 samples

Table 2 Electrical resistivity, carrier concentration and Hall mobility of the $(In_{1-x}Lu_x)_2O_3$ samples at 298K

Table 3 Carrier concentration of $In_{2-2x}Lu_{2x}O_3$(x=0, 0.05) under different treatment (Air, Ar and N_2) at 298K

Fig. 1 SEM images of thermally-etched undoped In_2O_3 samples prepared using co-precipitation method followed by (a) spark plasma sintering and (b) normal pressure-less sintering

Fig. 2 Temperature dependence of (a) electrical properties and (b) thermopower of Lu-doped In_2O_3 compounds (c) Electrical resistivity and the thermopower as a function of Lu doping concentration

Fig. 3 Temperature dependent power factor of $(In_{1-x}Lu_x)_2O_3$ ceramics

Fig. 4 Band gap energy as a function of Lu doping concentration at room temperature.

Fig. 5 Raman spectra of $(In_{1-x}Lu_x)_2O_3$ and Lu_2O_3 samples at room temperature.

Fig. 6 XRD patterns of the (In1-xLux) 2O3 samples. Insert: (222) peaks

Fig. 7 Temperature dependence of thermal conductivity for $(In_{1-x}Lu_x)_2O_3$ samples

Fig. 8 Temperature dependent ZT of $In_{2-2x}Lu_{2x}O_3$ ceramics

Table 1

Sample(x)	Mass Density(g/cm^3)	Relative density (%)
0	7.12	92
0.025	7.18	94
0.05	7.23	93
0.1	7.35	91
0.15	7.48	89

Table 2

x	ρ (Ω cm)	μ ($cm^2V^{-1}s^{-1}$)	n×10^{18} (cm^{-3})
0	0.010	92.5	7.01
0.025	0.021	106	2.79
0.05	2.740	10.8	0.21
0.1	2.251×10^3	0.3	0.0092
0.15	1.128×10^5	0.3	0.0002

Table 3

x	n(10^{18}cm^{-3})		
	Air	Ar	N_2
0	7.01	5.84	5.40
0.05	0.21	1.61	0.67

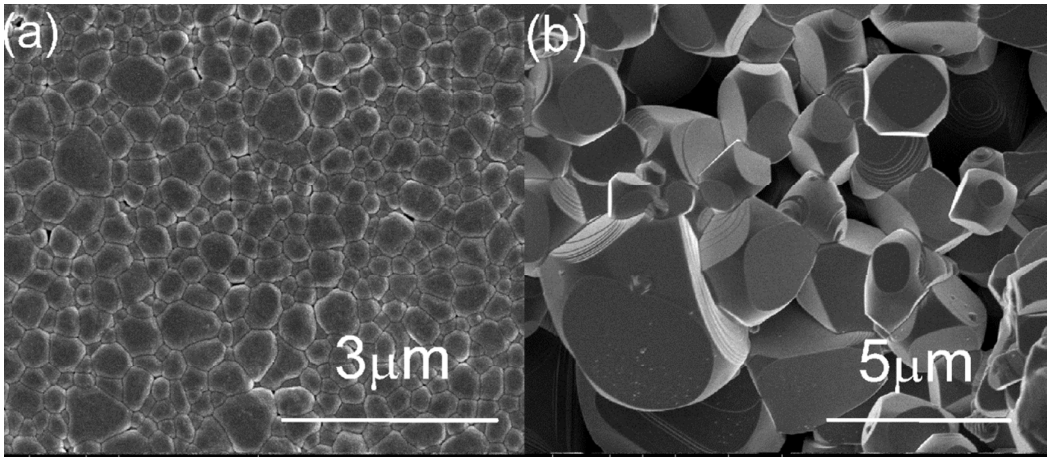

Fig. 1

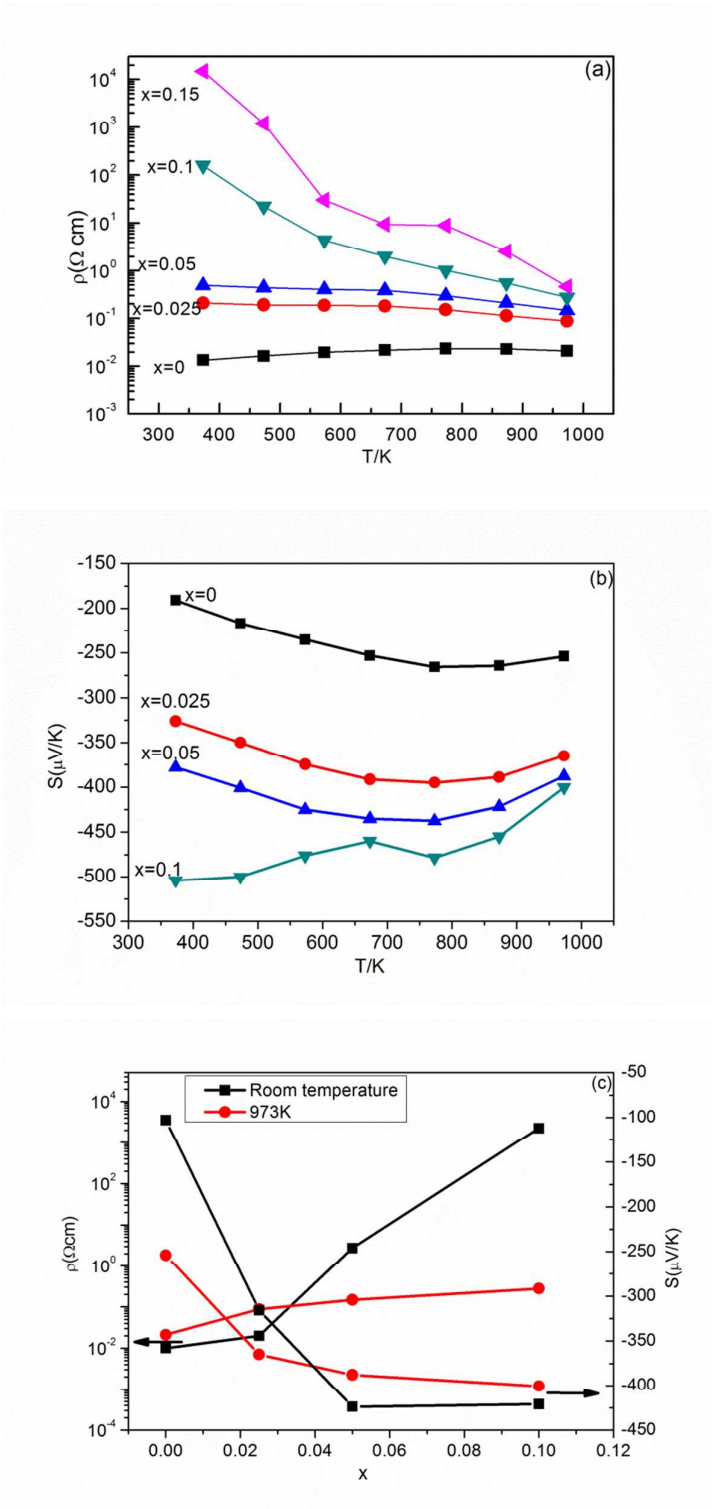

Fig. 2

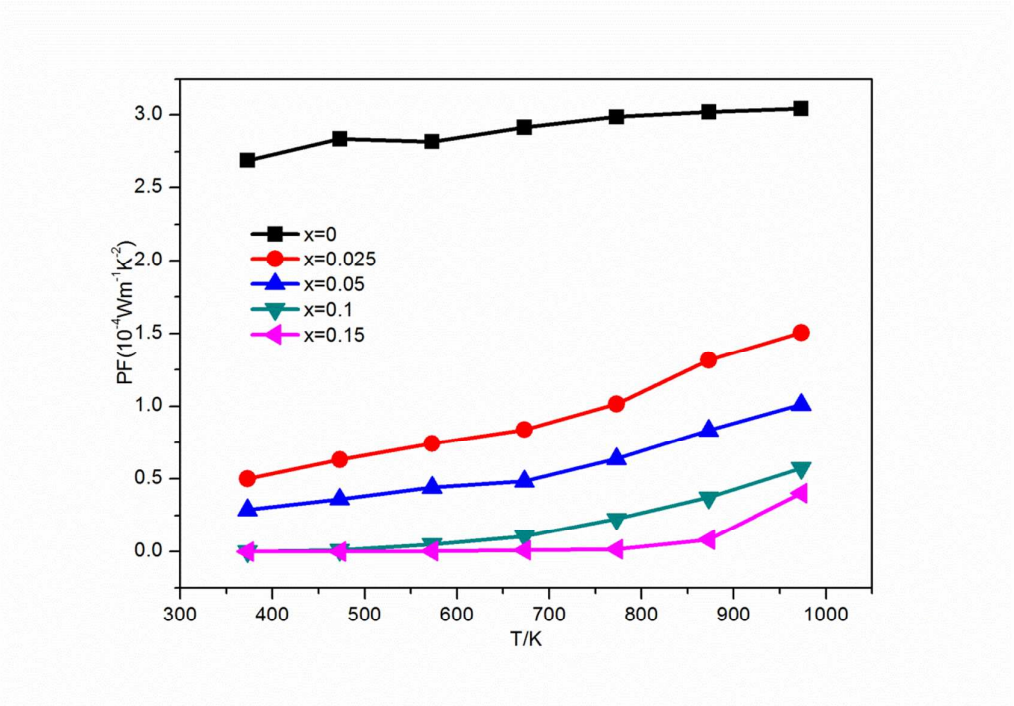

Fig. 3

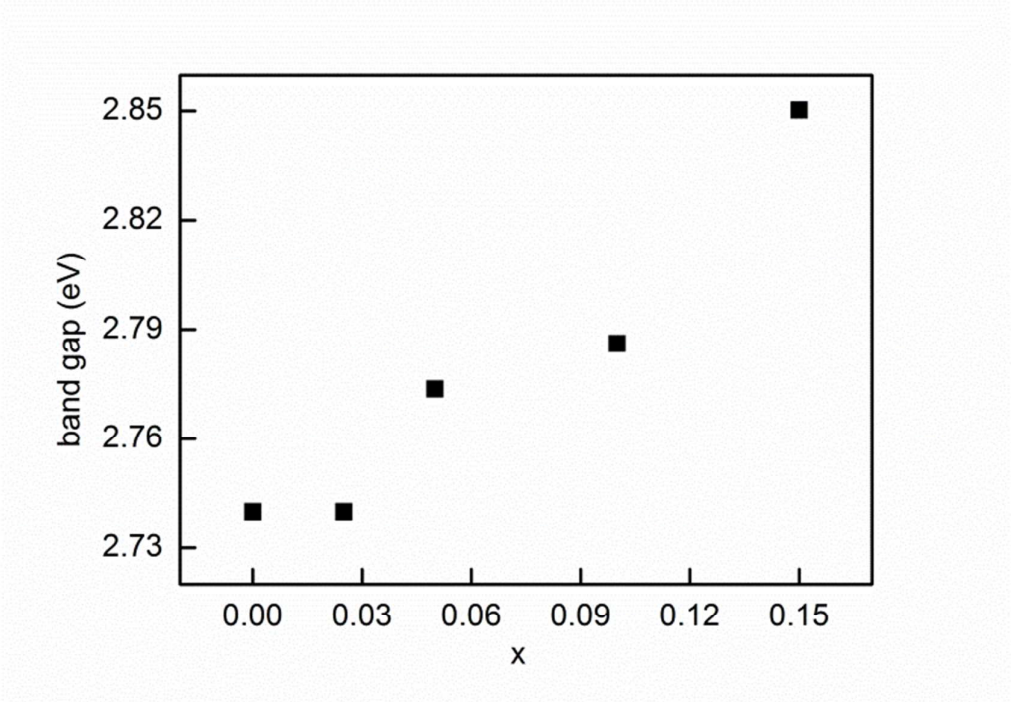

Fig. 4

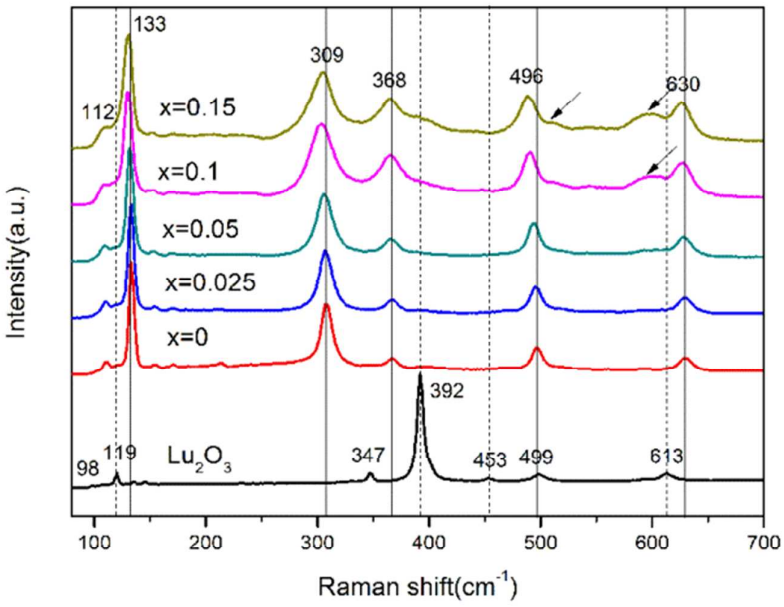

Fig. 5

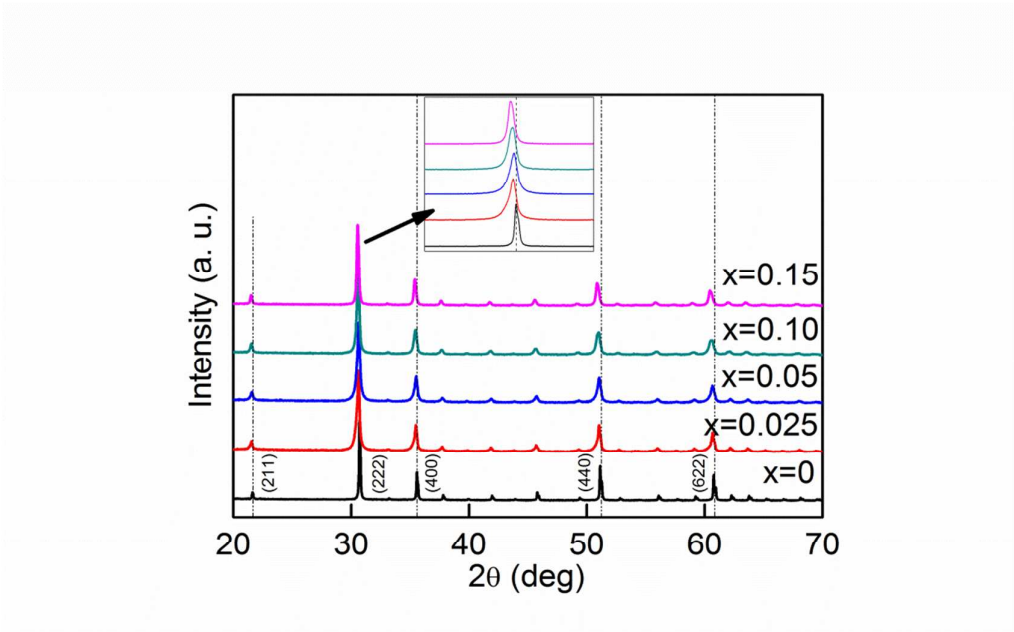

Fig. 6

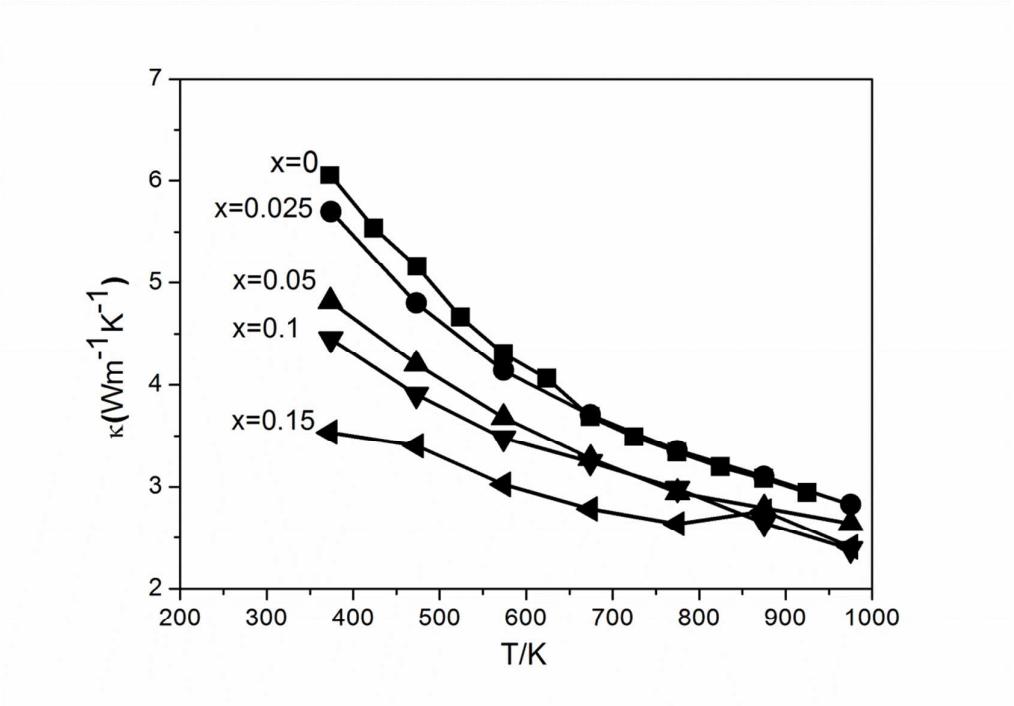

Fig. 7

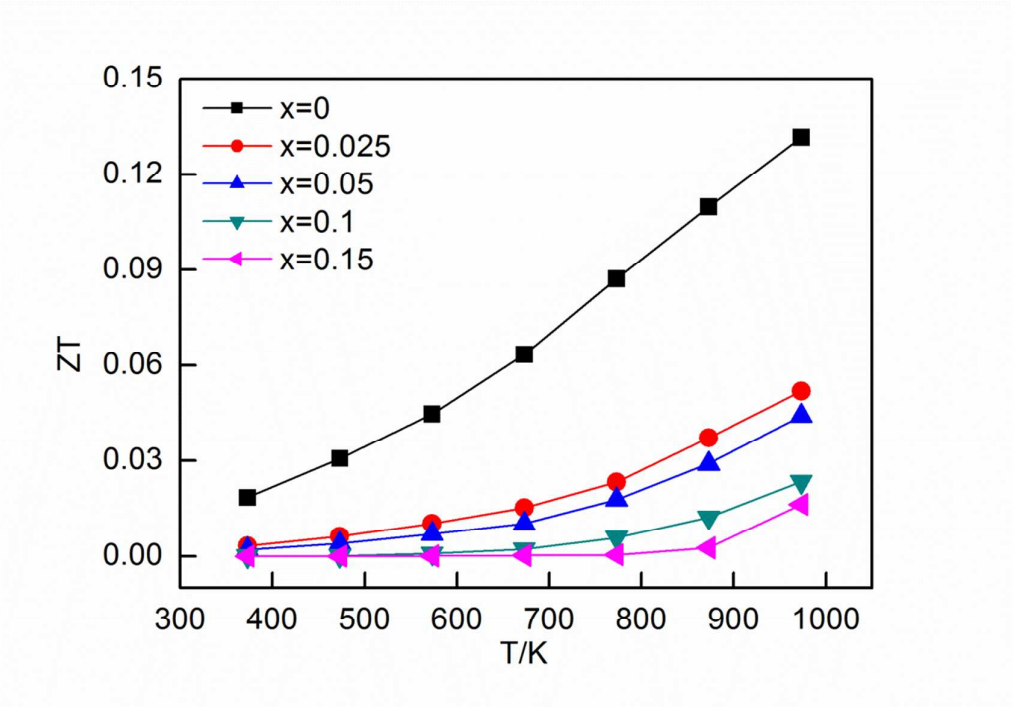

Fig. 8